Supporting Information

Yang et al.

SI Materials and Methods

Generation of Lrrc26 KO mice

Mice obtained from KOMP were bred with CMV-Cre deleter mice (B6.C-Tg(CMV-cre)1Cgn/J, The Jackson Laboratory) to delete the selection cassette. The *Lrrc26*$^{-/-}$ strain has been maintained in a C57BL/6 background out to N=6. All procedures related to animal care and treatment conformed to institutional and NIH guidelines. Genotyping of all animals was accomplished with PCR reactions on mouse tail samples, through a pair of PCR reactions. For the KO allele, the primer pairs were 5'AGAACTGGTGGCTTTGATCG and 5'-GTCTGTCCTAGCTTCCTCACTG, resulting in a 385 bp product (**Fig. S2B**), while, for the WT allele, the primer pairs were 5'-TCCGGATGCCGCCTTCAAACAGTG and 5'-GGAGCACTAGAAACAACCTGCAGT, resulting in a 290 bp product.

Bluo-Gal staining

Fresh tissues from *Lrrc26*$^{-/-}$ mice were dissected and quickly immersion-fixed with 0.2% glutaraldehyde in PBS buffer at 4^{o}C for 24 hours. Fixed tissues were transferred to ice-cold 30% sucrose in PBS buffer and kept at 4^{o}C for 24 hours. 20-25 µm frozen tissue sections were then prepared with cryostat at -20^{o}C. Slides were washed once briefly with PBS and then once with 37^{o}C Bluo-Gal dilution buffer (5 mM Potassium Ferricyanide, 5 mM Potassium Ferrocyanide, 2 mM Magnesium Chloride, 0.1% Tween-20 in PBS(pH 7.4)). Just before staining, Bluo-Gal stock solution (4% (w/v) Bluo-Gal (Invitrogen, 15519-028) in dimethylformamide) was diluted at 1:40 in 37^{o}C Bluo-Gal dilution buffer to prepare the fresh Bluo-Gal working solution. Tissue sections were then incubated in the Bluo-Gal working solution at 37^{o}C in a humidity box. In order to obtain clear and specific staining results, the staining times have been optimized as follows: 1-2 hours for lacrimal gland; 2-4 hours for submandibular gland, prostate and trachea; 3-4 hours for vomeronasal organ; 24 hours for all other tested tissues. Wild-type tissue sections were prepared and stained side by side with the same protocol as negative controls. Finally, sections were rinsed in PBS, counterstained with Eosin Y Solution (HT110116-500 ml; Sigma-Aldrich, St. Louis MO USA) or Periodic Acid-Schiff (PAS) Staining System (395B-1KT; Sigma-Aldrich) and mounted with aqueous mounting medium.

RNA extraction and quantitative RT-PCR

Tissues from C57BL/6J mice (8-12 weeks old) were dissected, quickly frozen in liquid nitrogen and, then saved at -80^{o}C. Total RNA from each tissue was isolated using the RNeasy Plus Mini Kit (Qiagen, Valencia, CA USA). cDNA was synthesized using the BioRad iScript cDNA Synthesis Kit (170-8891; BioRad, Hercules, CA USA). For the negative control groups, all components except the reverse transcriptase were included in the reaction mixtures. Real-Time PCR was performed with specific primers (**Table S1**) and Power SYBR Green PCR Master Mix (Applied Biosystems, Waltham MA, USA; 4367659) under reaction conditions identical to that described previously (1). PCR specificity was verified by the dissociation curve from a single peak which was run following the real-time PCR reaction. Message levels were normalized to

the abundance of β-actin message. The mean value was averaged from 3 separately prepared RNA samples.

Table S1 Primers used for real-time PCR

mouse gene	Cat.No. of QuantiTect Primer Assay from Qiagen	amplicon length (bp)
Kcnma1	Forward: 5'-TCTCAGCATTGGTGCCCTCGTAAT-3' Reverse: 5'-GTAGAGGAGGAAGAACACGTTGAA-3'	127
Lrrc26	Forward: 5'-TGTGCGCTGCGTCCCCTTTGCACT-3' Reverse: 5'-CGGCATCCGGAAAAGCTGTCAGTA-3'	127
β-actin	Forward: 5′-TGGAGAAGAGCTATGAGCTGCCTG-3′ Reverse: 5′-GTAGTTTCATGGATGCCACAGGAT-3′	127

Note: All the above primers amplify regions crossing adjacent exons.

Protein preparation, Immunoprecipitation, Protein Deglycosylation and Western Blotting

Mouse tissues from 8-12 week old mice were frozen in liquid nitrogen, smashed into powder with the liquid nitrogen pulverizer and then homogenized on ice with a Teflon-glass pestle in 0.32 M sucrose in PBS solution, including 10 mM PMSF in acetone and 1%(v/v) Protease Inhibitor Cocktail (P8465-25ml, Sigma-Aldrich). The tissue suspension was centrifuged at 300 g for 10 minutes at 4°C and the supernatant was then transferred to an ultra-speed centrifuge tube. The membrane faction was isolated by centrifuging the tube at 150,000 g for 60 minutes and the resulting membrane pellet was resuspended in 1% dodecyl maltoside (DDM) lysis buffer (50 mM Na phosphate, 150 mM NaCl, 10 mM KCl, 1% DDM, pH 7.2) with 10 mM PMSF in acetone and 1% (v/v) Protease Inhibitor Cocktail. The suspension was rocked in a 4°C cold room for 2 hours and then centrifuged at 18,000 g for 10 minutes. The supernatant was saved as the membrane protein sample. 1.5 ml of membrane proteins was mixed with 4 μg of a custom polyclonal rabbit anti-mLRRC26 antibody (Prosci Inc., Poway, CA USA) and 30 μl Trueblot Rabbit IP beads (00-8800-25; Rockland Immunochemicals, Limerick, PA USA) at 4^{o}C for overnight. The rabbit anti-LRRC26 antibody was raised to an epitope near the LRRC26 C-terminus corresponding to residues 299-320: RTTVRHLLRRQLDPEGPPSLED. IP Beads were collected by a brief spin at 10,000 g, washed thrice, and finally resuspended in 37.5 μl of 0.5% DDM lysis buffer. To remove the N-linked glycosylated sugars in the IP product, 1 μl of PNGase F (170-6883; Bio-Rad) was used according to manufacturer's non-denaturing protocol. The deglycosylation reaction was done at 37 ^{o}C for 1 hour. Proteins were then eluted from beads at room temperature for 30 minutes by the addition of 25 μl Laemmli SDS-Sample Buffer (BP-110R, Boston BioProducts, Ashland, MA USA) to each 50 μl reaction mixture. Western blots were performed as previously described (2). For the primary Abs, anti-SLO1 (L6/60; Antibodies Inc., Davis, CA USA) was diluted to 2 μg/ml in 5 ml 0.25% non-fat milk in PBS (0.1% Tween 20); anti-mLRRC26 (ProSci) was diluted to 2.8 μg/ml in 5 ml 0.25% non-fat milk in PBS (0.1% Tween 20); Sodium Potassium ATPase Alpha 1 Antibody (M7-PB-E9) (#NB300-584, Novus Biologicals, Littleton, CO USA) was diluted to 10 μg/ml in 5 ml 0.25% non-fat milk in PBS (0.1% Tween 20). For secondary antibodies, Mouse TrueBlot Ultra anti-mouse IgG HRP (18-8817-33, Rockland) and Rabbit TrueBlot Ultra anti-rabbit IgG HRP (18-8816-33, Rockland) were 1:2500 diluted in 5 ml 0.25% non-fat milk in PBS (0.1% Tween 20), respectively.

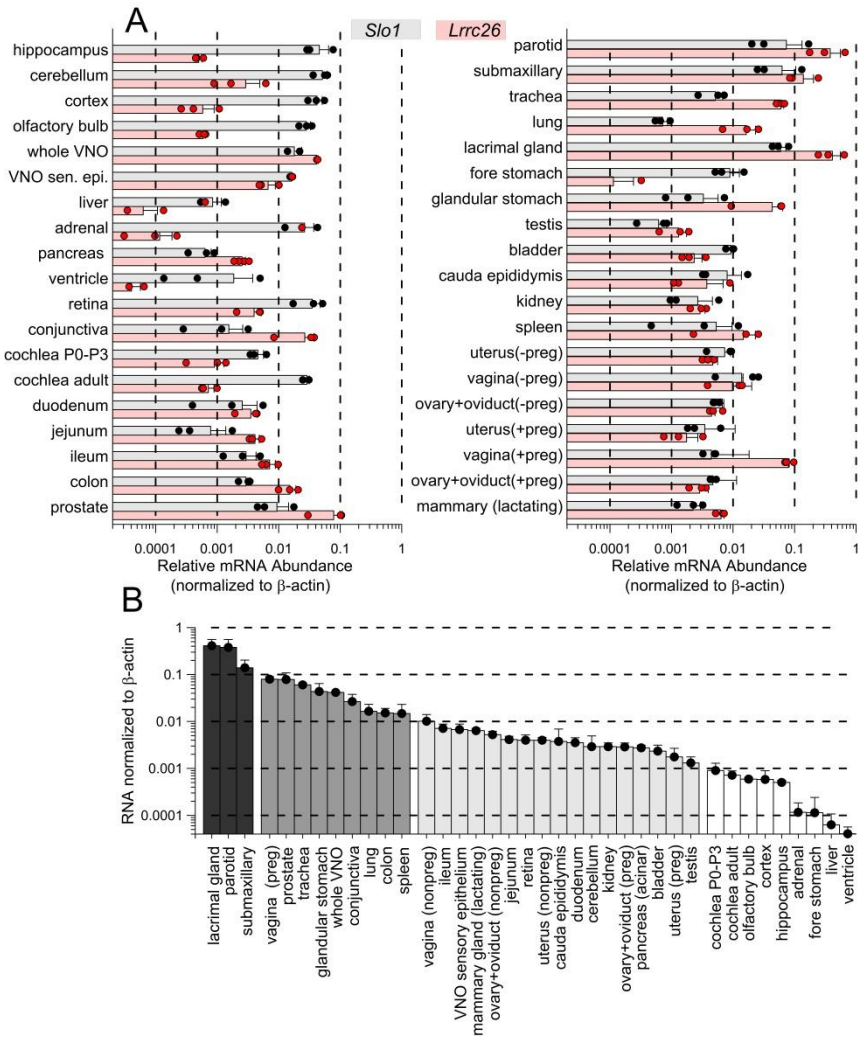

Fig. S1. Quantitative RT-PCR of mouse tissues for presence of *Kcnma1 (Slo1)* and *Lrrc26* message. (A) For each indicated tissue, three separate RNA preparations (except for whole VNO where n=2) were prepared and each sample run in triplicate. Bars show means and standard errors, while means from individual preparations are given by filled circles. All values for both *Slo1 (Kcnma1*; gray) and *Lrrc26* (red) were normalized to the abundance of β-actin message. (B) Levels of *Lrrc26* message relative to β-actin are plotted in order of relative abundance with bars shaded for measurements within each 10-fold level of expression.

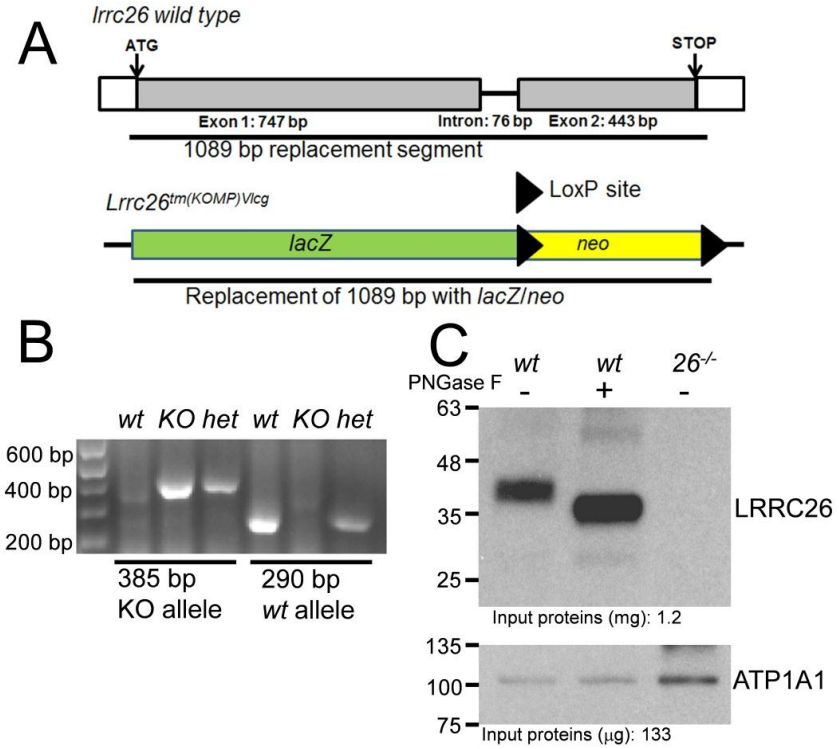

Fig. S2. Generation and confirmation of LRRC26 KO. (A) The wild type *Lrrc26* genomic structure is shown. The gene contains two exons with a short intron. 1089 base pairs (nucleotides 25289972-25291060 in mouse chromosome 2) in the wild type gene were replaced with sequence encoding *lacZ* and a neomycin-resistance (*neo*) cassette with the latter bracketed by LoxP sites (shown on bottom). The 5' insertion of the *lacZ* gene is 17 nucleotides before the original start codon of the *Lrrc26* gene and is expected to be under control of the *Lrrc26* promoter. Mice heterozygous for the KO allele were obtained following resuscitation of cryopreserved embryos from the KOMP repository. The floxed neomycin cassette was subsequently deleted in crosses with CMV-Cre deleter mice (B6.C-Tg(CMV-cre)1Cgn/J, The Jackson Laboratory). (**B**) PCR reactions from mouse tails confirm the successful disruption of the *Lrrc26* coding region. Each tail sample was used in two separate PCR reactions. Left three lanes show a PCR reaction to test for a 385 bp product corresponding to the *Lrrc26* KO allele, while right three lanes test for presence of 290 bp *wt* allele. (**C**) Membrane proteins from prostate were purified and subjected to immunoprecipitation with the LRRC26 Ab. (Top) Following western blot, the LRRC26 polyclonal Ab (ProSci) identifies a band of about 40 kD in *wt* samples, a 35 kD band following deglycosylation with PGNase F, and the absence of any band in the *Lrrc26*$^{-/-}$ mice. (Bottom) Total membrane protein samples were blotted with Na^+/K^+ ATPase Alpha1 Ab (ATP1A1; Novus). Note increase in ATP1A1 in the *Lrrc26*$^{-/-}$ sample. This was also seen in other tissues (e.g,. trachea, mammary gland, lung, and glandular stomach (Fig. 1)). We have no explanation for this. Although ATP1A1 is a typical control marker in membrane protein samples, it is possible that its abundance can be regulated. The increased intensity in the ATP1A1 band does not alter the conclusion that LRR26 protein is absent in the KO tissues.

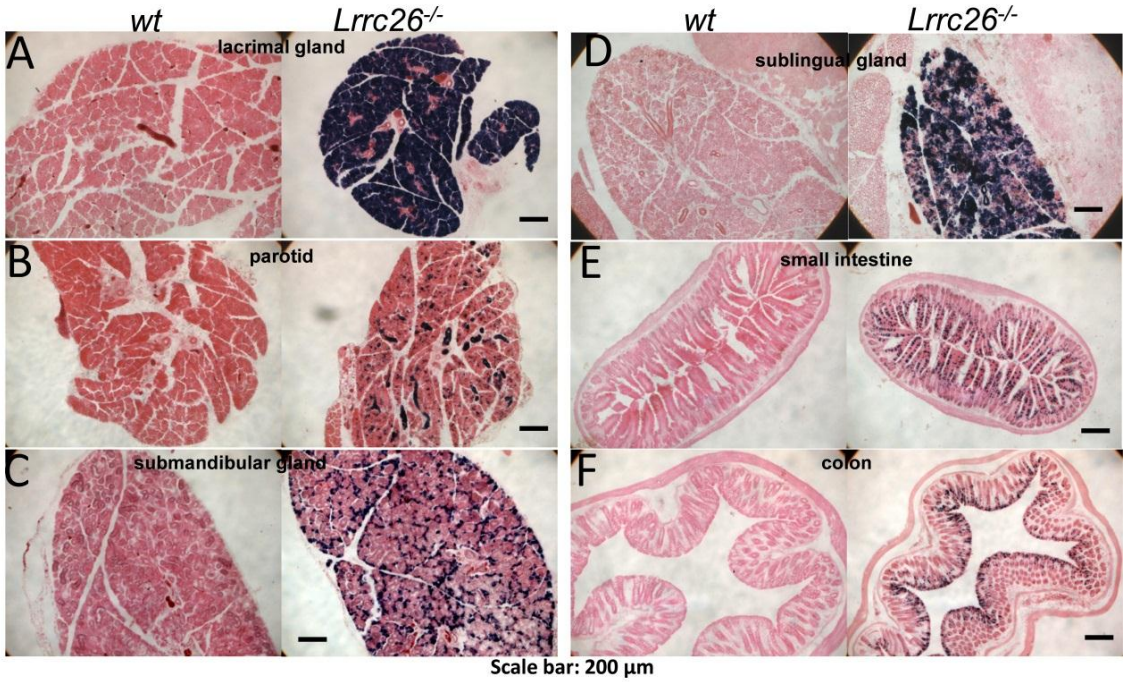

Figure S3. Representative low resolution views of glandular and intestinal tissues showing positive Bluo-Gal reaction product in the LRRC26 KO mice. In all cases, 20 µm sections were obtained. Tissue-specific details of the fixation and Bluo-Gal reaction incubation conditions are given in the Methods. Tissues include: (A) lacrimal gland, (B) parotid, (C) submandibular gland, (D) sublingual gland, (E) small intestine, and (F) colon.

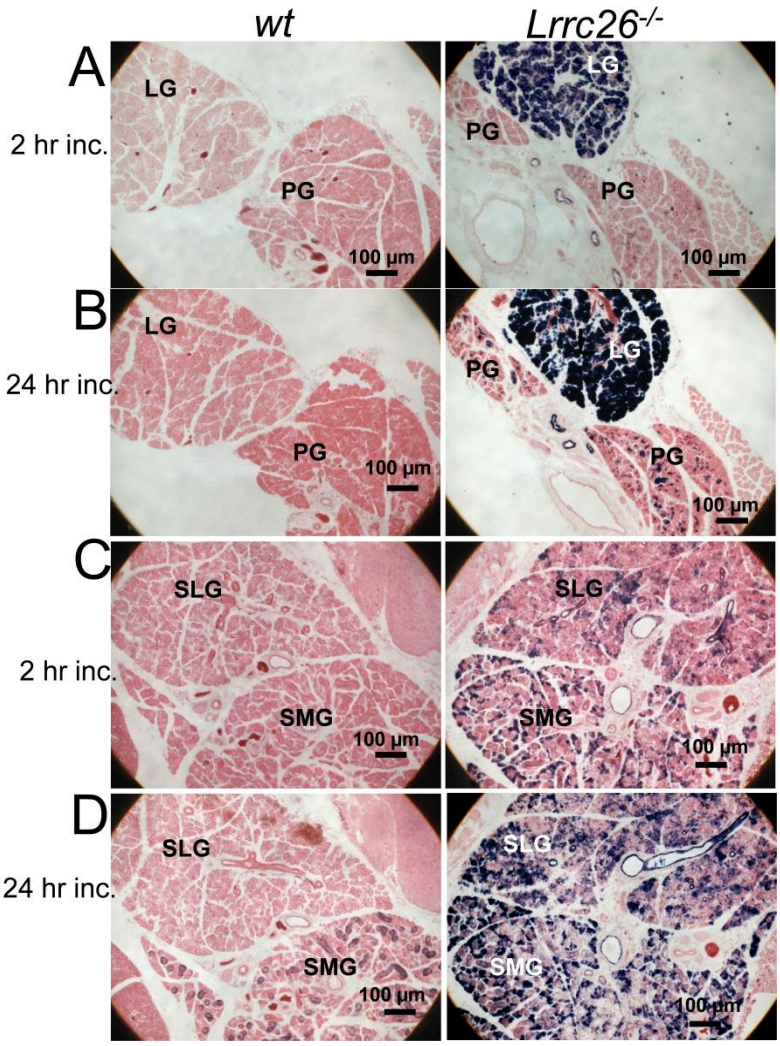

Figure S4. Comparison of lacrimal and parotid gland Bluo-Gal staining in the same sections highlights tissue-specific variation in effectiveness of Bluo-Gal reaction. (A) Left panel shows a section through both lacrimal (LG) and parotid gland (PG) from a *wt* mouse following a 2 hour Bluo-Gal incubation, while, on the right, a section from an LRRC26 KO mouse that also shows both lacrimal and parotid glands was also subjected to a 2 hour Bluo-Gal incubation. (B) Left and right hand panels correspond to sections from *wt* and LRRC26 KO mice, again showing both lacrimal and parotid gland, but incubated in the Bluo-Gal working solution for 24 hours. The factors influencing tissue-specific differences in the Bluo-Gal reaction despite ostensibly similar message levels in *wt* tissues remain unknown. (C) Sections show comparison of *wt* (left) and LRRC26 KO (right) Bluo-Gal staining of sublingual gland (SLG) and submandibular gland (SMG) following 2 hours incubation in Bluo-Gal working solution.(D) Sections compare *wt* and LRRC26 KO staining in sublingual and submandibular glands after 24 hours incubation. Note that ductal cells in the submandibular gland exhibit dark appearance in *wt* sections after 24 hrs incubation.

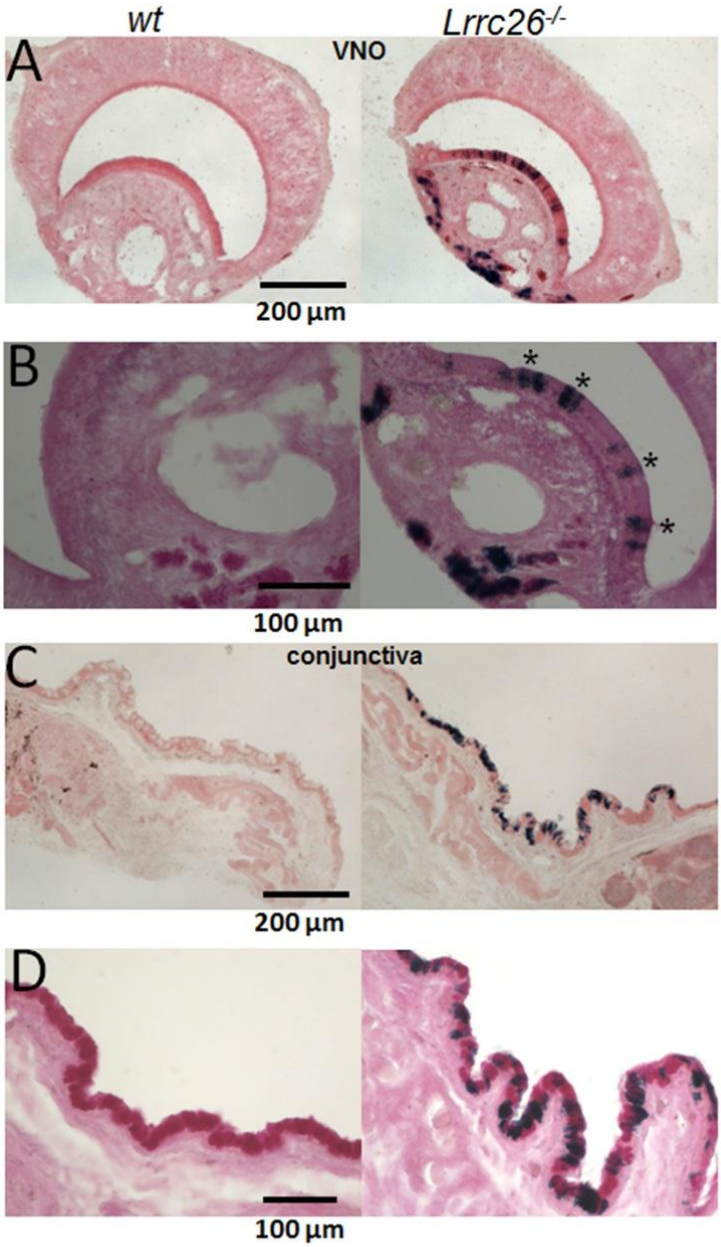

Figure S5. PAS-positive, Bluo-Gal positive cells are also found in VNO and conjunctiva. (A) Lower resolution view of VNO section shows that Bluo-Gal positive cells in non-sensory epithelium and also other cells adjacent to lumen in the *Lrrc26*$^{-/-}$ section (right), but not in *wt* (left). (B) On the left, higher resolution VNO section shows clumps of PAS-positive cells corresponding to cells of Jacobson's glands from a *wt* mouse . On the right, PAS-positive cells overlap with Bluo-Gal positive cells from a section from *Lrrc26*$^{-/-}$ mouse. Also note Bluo-Gal staining in the non-sensory epithelium (*). (C) Bluo-Gal straining is also observed in the epithelial cell layer of *Lrrc26*$^{-/-}$ conjunctiva (right), but not in *wt*. (D) The *wt* conjunctiva epithelial layer exhibits robust PAS staining, which overlaps with Bluo-Gal staining in the *Lrrc26*$^{-/-}$ conjunctiva.

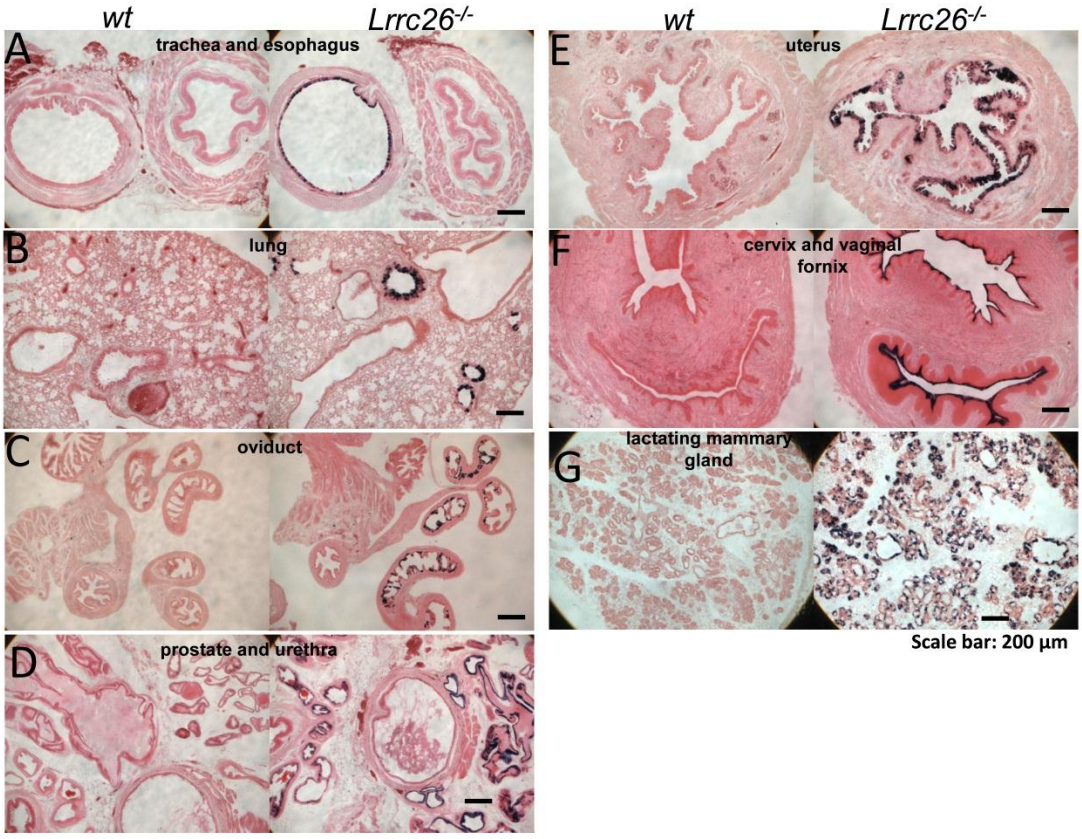

Figure S6. Epithelial cell layers in other tissues show dark blue Bluo-Gal staining in the LRRC26 KO mice. As before, tissue-specific details of the fixation and Bluo-Gal reaction incubation conditions are given in the Methods. Tissues positive for Bluo-Gal staining in the LRRC26 KO mice, but not *wt*, include: (A) trachea (esophagus is negative), (B) bronchioles in lung, (C) oviduct, (D) prostate(urethra is negative), (E) uterus, (F) cervix and vaginal fornix, and (G) lactating mammary gland.

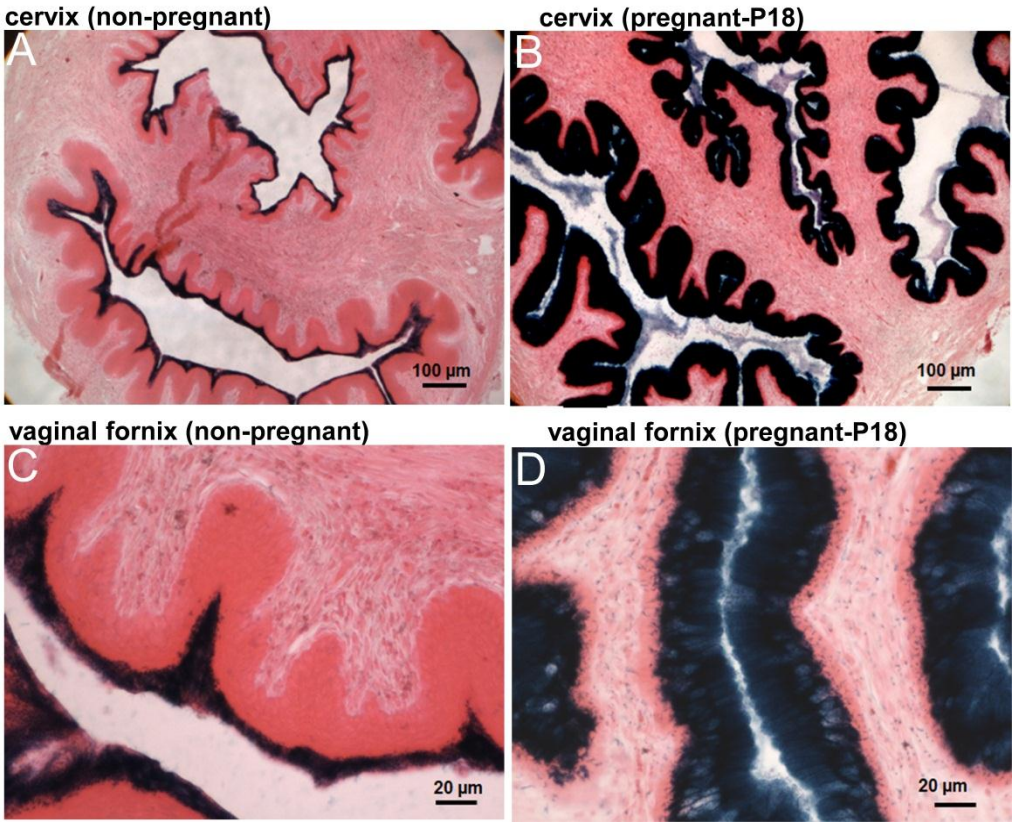

Figure S7. Epithelia cell layers in cervix and vagina exhibit enhanced Bluo-Gal staining during pregnancy. (A) Cervical section from non-pregnant *Lrrc26*$^{-/-}$ female. (B) Similar cervical section from a pregnant *Lrrc26*$^{-/-}$ female at P18. (C) Higher magnification section showing vaginal fornix from a non-pregnant *Lrrc26*$^{-/-}$ female. (D) Section of vaginal fornix from P18 *Lrrc26-/-* female.

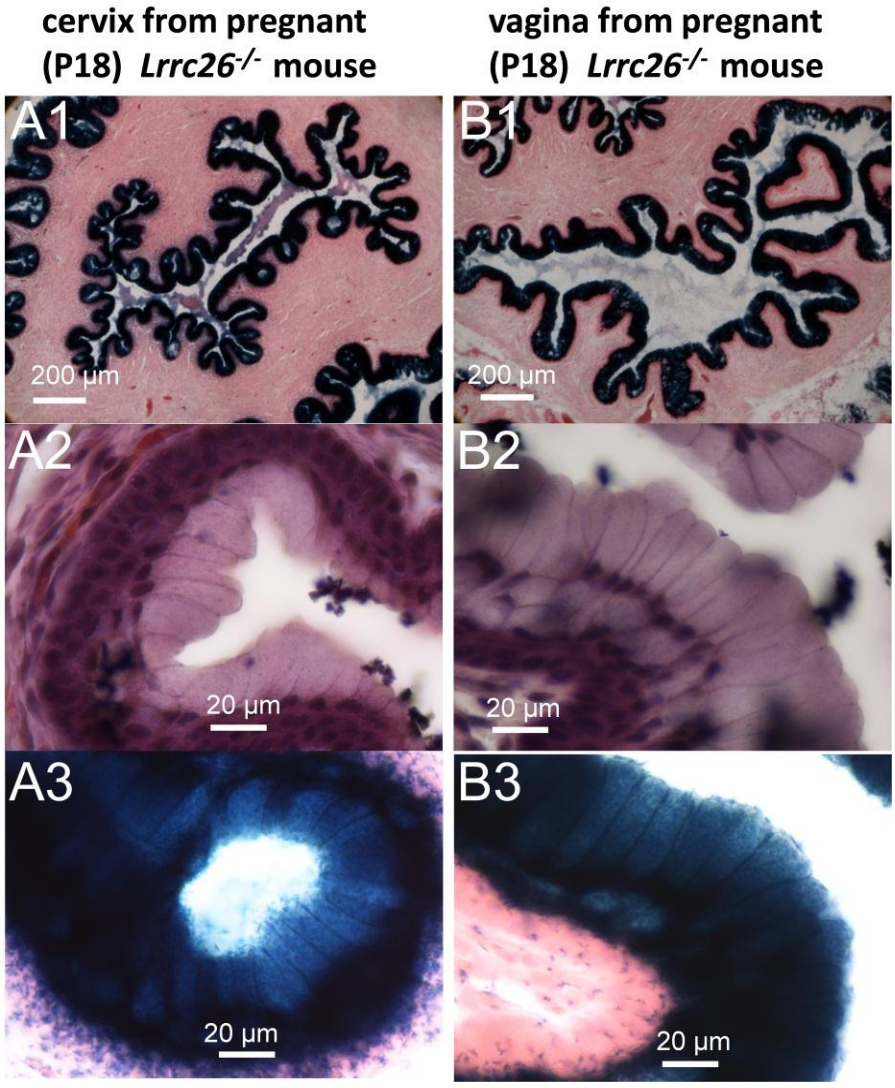

Figure S8. Higher magnification views of pregnant cervix and vagina reveal Bluo-Gal staining in superficial columnar epithelial cells. (A1-A3) Sections from cervix of P18 *Lrrc26*$^{-/-}$ female showing low resolution view (A1) of Bluo-Gal staining with eosin counterstaining, higher resolution hematoxylin/eosin stained view (A2) showing superficial columnar epithelial cells, and then a similar view of the columnar epithelial layer with strong Bluo-Gal staining (A3). (B1-B3) Sections from vagina of P18 *Lrrc26*$^{-/-}$ female show lower resolution view (B1), higher resolution view (B2) showing large columnar epithelial cells, and then the Bluo-Gal staining (B3) in the epithelial layer.

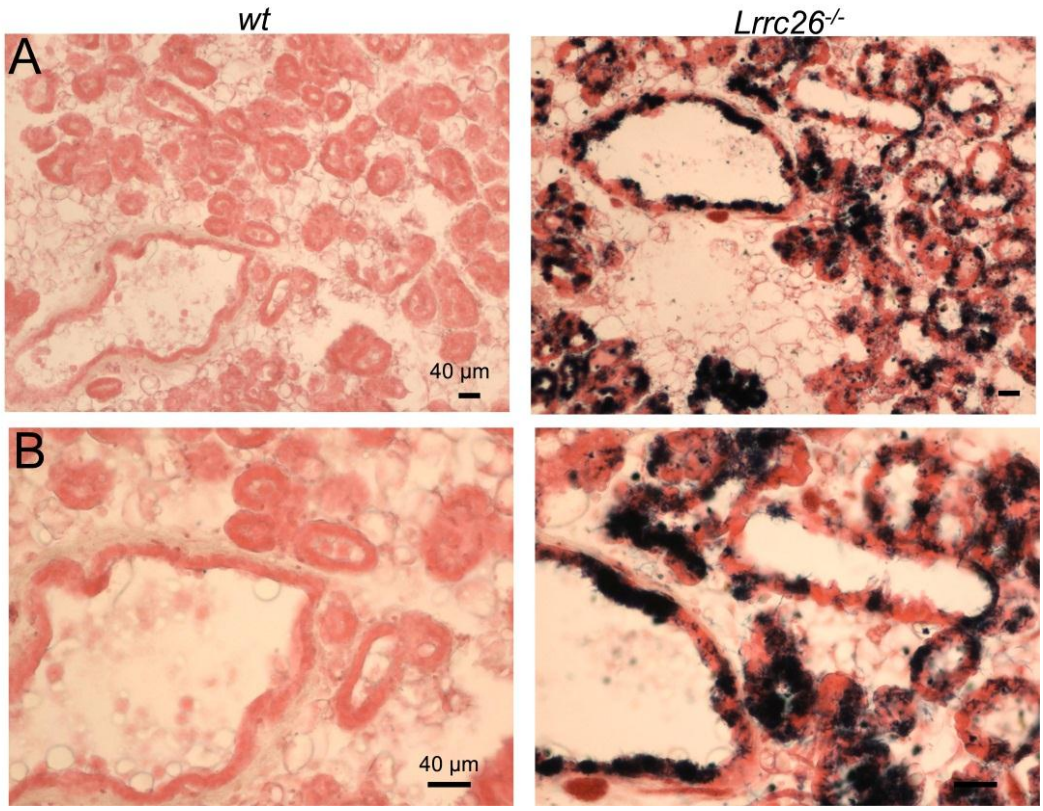

Figure S9. Bluo-Gal staining in lactating mammary gland is associated with alveoli and cells lining ducts. (A) On the left, section (10x) from a *wt* lactating mammary gland is negative for Bluo-Gal reaction product, while, on the right, sections from *Lrrc26*$^{-/-}$ lactating mammary gland reveal Bluo-Gal positive cells surrounding ducts and also in cells likely to contribute to alveoli. **(B)** Left and right panels are as in A, but at 20X magnification to better highlight the loci of Bluo-Gal staining.

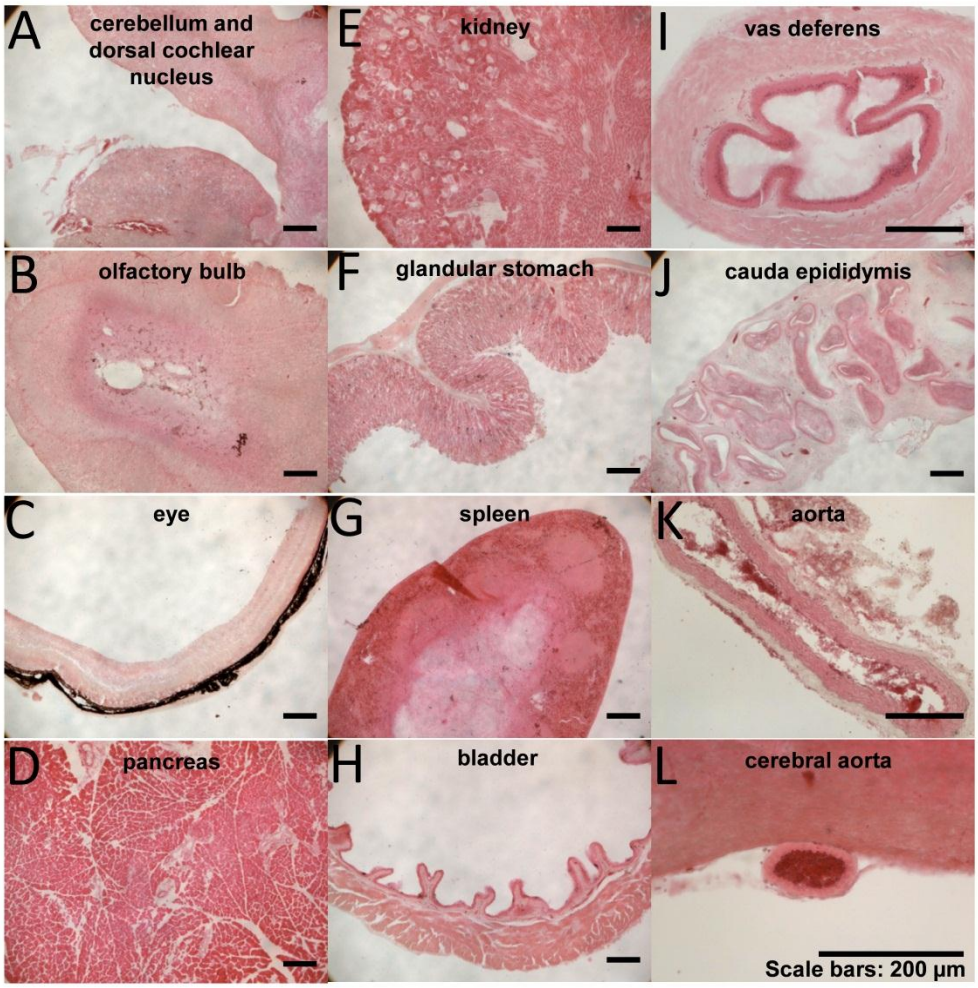

Figure S10. Tissues from *Lrrc26*$^{-/-}$ mice that are negative for Bluo-Gal staining. Tissues for which Bluo-Gal staining was undetectable and indistinguishable between LRRC26 KO and *wt* included: (A) cerebellum and dorsal cochlear nucleus, (B) olfactory bulb, (C) eye, (D) pancreas, (E) kidney, (F) glandular stomach, (G) spleen, (H) bladder, (I) vas deferens, (J) cauda epididymis, (K) aorta, and (L) cerebral aorta.

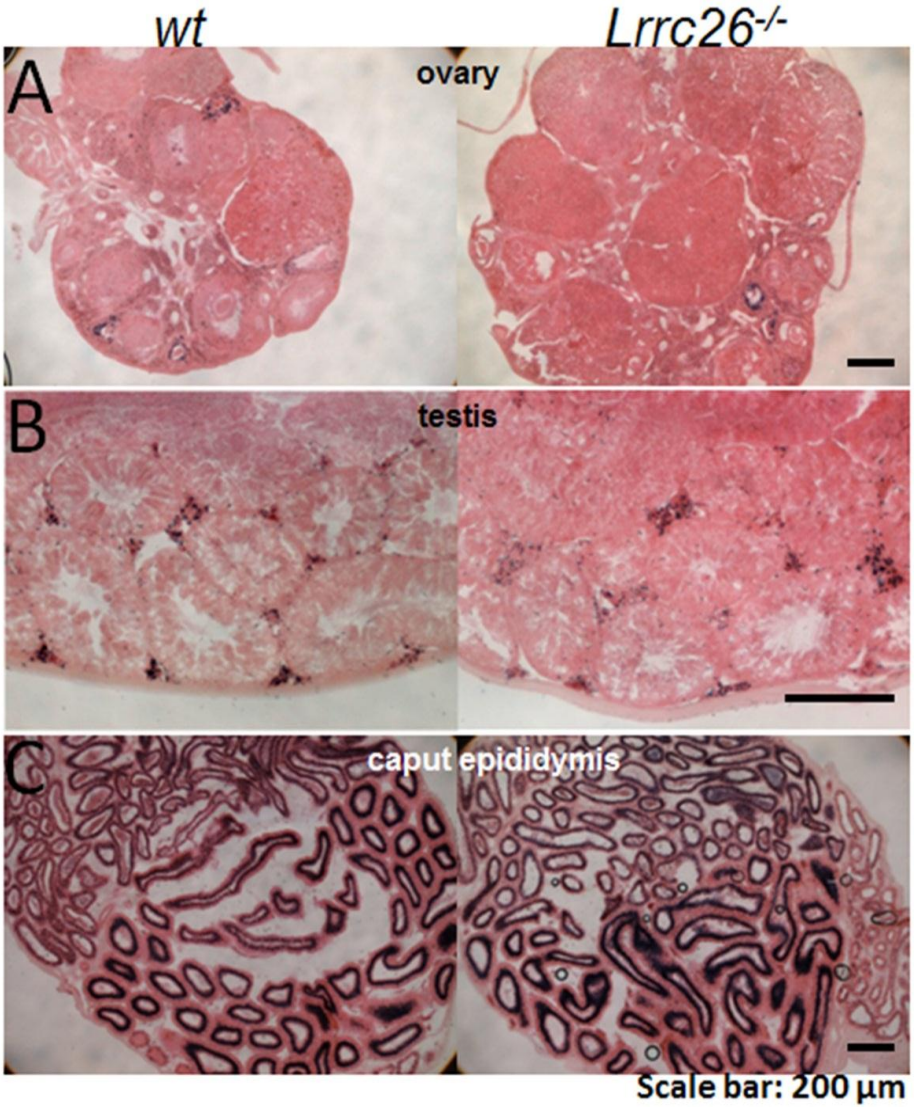

Figure S11. Tissues for which nonspecific dark staining was observed in both *wt* and *Lrrc26*$^{-/-}$ mice. (A) Tissues were first developed for Bluo-Gal staining and then counterstained with eosin. In sections of ovary from both *wt* and *Lrrc26*$^{-/-}$ mice, loci of somewhat darkened tissue were observed which did not differ between genotypes. (B) Sections from both *wt* and *lrrc26*$^{-/-}$ testis also show similar darkened loci, with no indication of any specific Bluo-Gal staining. (C) Sections from caput epididymis also exhibit similar dark loci that are identical between *wt* and KO mice.

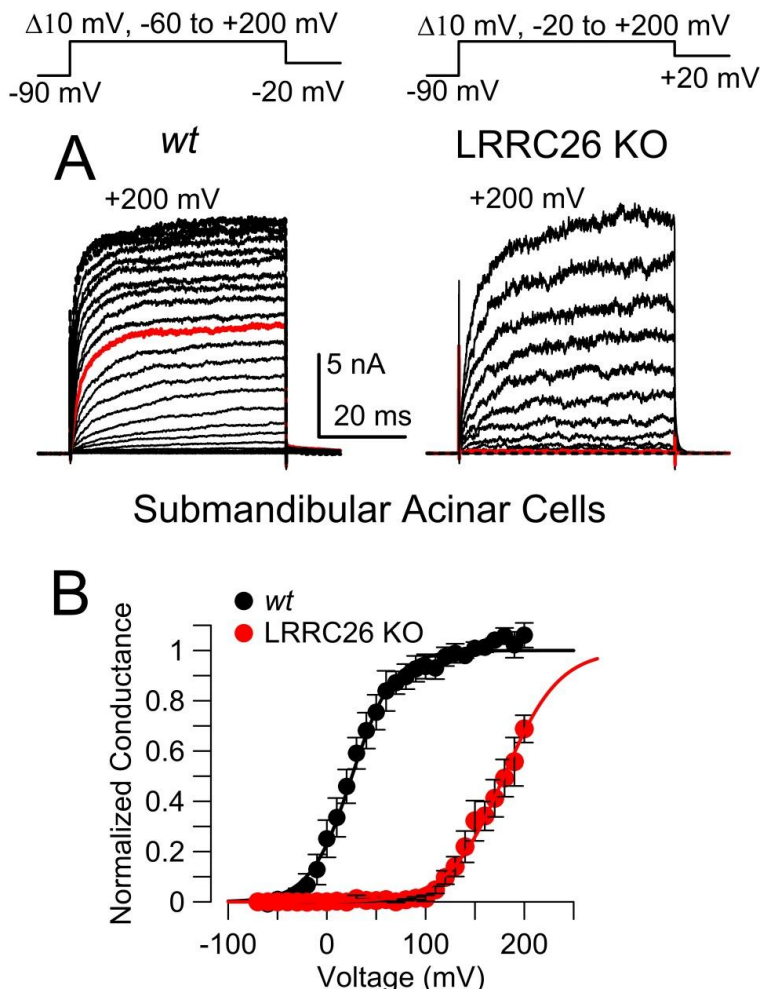

Figure S12. KO of LRRC26 shifts gating of BK currents in submandibular acinar cells. A) Currents (shown to +200 mV) were activated with the indicated voltage protocol in a *wt* acinar cell (left) and an LRRC26 KO acinar cell (right) from submandibular gland. Pipette/intracellular Ca^{2+} was 250 nM. Red trace reflects voltage step to +100 mV. (B) GV curves were generated from tail currents recorded from traces as in panel A. From fits to individual cells, for 5 *wt* cells, mean V_h = 25.7±6.3 mV and z=1.4±0.2e; for 5 LRRC26 KO cells, V_h = 169.2±9.6 mV with z=1.3±0.1e. Fits of averaged GVs yielded similar values: for *wt*, V_h=25.4±1.7 mV (±90% c.l.) with z=1.5±0.09e and, for LRRC26 KO, V_h=179.4±1.5 mV with z=0.9±0.1e. Note that the GV from *wt* cells exhibited an upward climb at the most positive activation potentials. This was not observed in parotid or lacrimal gland cells. A two component Boltzmann function yielded a better fit to the *wt* GV curves (not shown), with the 2nd component approximating about 0.05 of the total conductance. We suggest that this may represent a fraction of BK channels without LRRC26 subunits, as has been noted in heterologous expression studies of LRRC26 with SLO1 subunits (3).

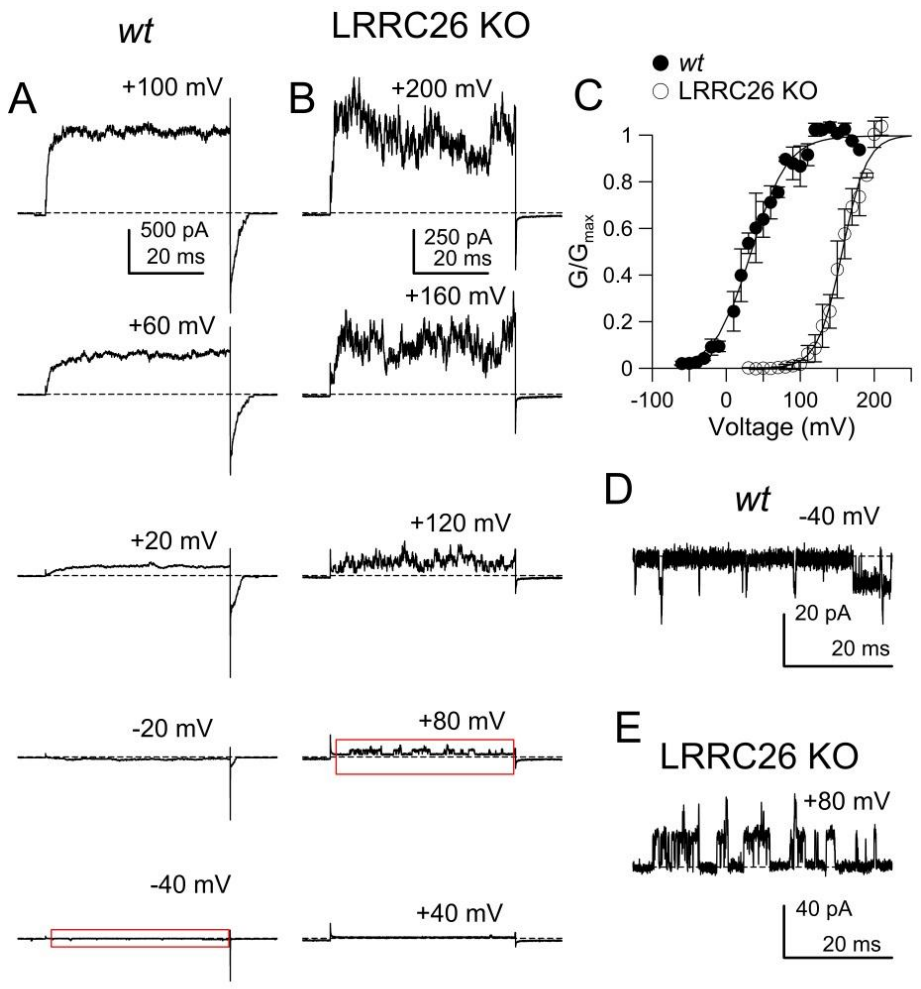

Figure S13. Excised inside-out patches of BK channel activity also reveal gating shift differences between *wt* and LRRC26 KO animals. (A) BK channels were activated in inside-out patches from a *wt* parotid cell with symmetric K^+ solutions and 0 cytosolic Ca^{2+}. Robust channel activation occurs at voltages negative to +50 mV. Red boxes highlight traces displayed at higher resolution in panels D and E. (B) BK channels from an inside-out patch from a LRRC26 KO parotid cell with 0 cytosolic Ca^{2+} require voltages in excess of +100 mV to produce appreciable channel activation. (C) GV curves were generated from measurements of steady-state current from BK channel activity from inside-out patches from 3 *wt* and 3 LRRC26 KO BK parotid cells. For *wt*, V_h=38.7±5.1 mV, z=1.01±0.03e; for LRRC26 KO, V_h=156.9±7.6 mV, z=1.6±0.1e. (D) Trace shows characteristic BK channel activity monitored at -40 mV in a patch from a *wt* parotid cell. (E) Trace shows openings of individual BK channels at +80 mV in a parotid cell patch from a LRRC26 KO mouse.

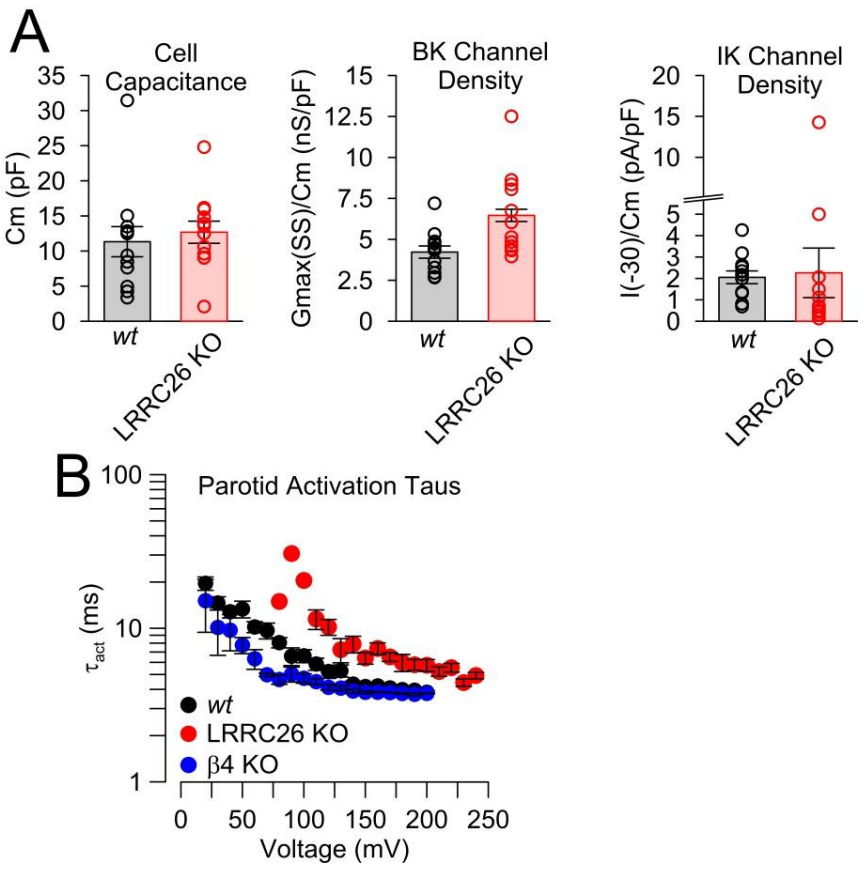

Figure S14. Comparison of basic properties of *wt* and LRRC26 KO parotid cells. (A) On the left, cell capacitance (Cm) is compared for 10 *wt* and 10 LRRC26 KO parotid cells. The KS test statistic yielded P= 0.186. In the middle, maximum BK conductance is compared for *wt* and LRRC26 KO cells. KS P= 0.066. On the right, IK current density estimated from current amplitude at -20 mV is compared for *wt* and LRRC26 KO parotid cells. KS P=0.433. **(B)** Time constants of activation were measured from 12 *wt*, 12 LRRC26 KO, and 3 β4 KO parotid cells.

References

1. Yang CT, Zeng XH, Xia XM, & Lingle CJ (2009) Interactions between beta subunits of the KCNMB family and Slo3: beta4 selectively modulates Slo3 expression and function. *PloS one* 4(7):e6135.
2. Yang C, Zeng XH, Zhou Y, Xia XM, & Lingle CJ (2011) LRRC52 (leucine-rich-repeat-containing protein 52), a testis-specific auxiliary subunit of the alkalization-activated Slo3 channel. *Proceedings of the National Academy of Sciences of the United States of America* 108(48):19419-19424.
3. Gonzalez-Perez V, Xia XM, & Lingle CJ (2014) Functional regulation of BK potassium channels by gamma1 auxiliary subunits. *Proceedings of the National Academy of Sciences of the United States of America*.